THE UNIVERSITY OF KANSAS CENTER FOR RESEARCH, INC.

2291 Irving Hill Drive—Campus West
Lawrence, Kansas 66045

THE QUASI-VORTEX-LATTICE METHOD FOR WINGS WITH EDGE VORTEX SEPARATION

by

Jenn-Louh Pao and C. Edward Lan

CRINC-FRL-385-1

January, 1980

The Flight Research Laboratory
The University of Kansas Center for Research, Inc.
The University of Kansas
Lawrence, Kansas 66045

A Final Technical Report
Prepared under NASA Grant NSG 1537:

"Investigation of Optimum Wing Configurations with Edge Separation"

for

Langley Research Center
National Aeronautics and Space Administration

Summary

In this investigation, the quasi-vortex-lattice method is used to predict the aerodynamic characteristics of wings with leading-edge vortex separation. The method is based on a flow model with free vortex elements which are allowed to merge into a concentrated core. The calculated pressure distribution is more accurate than that predicted by methods with discrete vortex filaments alone. In addition, the computer time is reduced approximately by half.

1. Introduction

Recently, lifting-surface methods have been applied to the calculation of wing aerodynamics with edge vortex separation. Two popular methods are of the doublet-panel type (Refs. 1 and 2) and the free vortices (Refs. 3 and 4). The panel method can predict accurate results. However, the computing time involved is lengthy and it has not been extended to treat complex geometries, such as wings with strakes and interacting surfaces. On the other hand, it is easier to extend the method of free vortices to complex geometries. However, the predicted pressure distribution is not accurate. In addition, the leading-edge Kutta condition is not exactly satisfied in the method of Ref. 3.

In Ref. 4, the quasi-vortex-lattice method was used, together with discrete vortex filaments to model vortex flow effects. The leading-edge Kutta condition is exactly satisfied and partial vortex separation is allowed. But the predicted ΔC_p distribution is more "diffused" than the data show. This is because the effect of a concentrated vortex core in the real flow cannot be accurately represented by a number of free vortices. The objectives of this investigation are to improve the pressure prediction of Ref. 4 by introducing a concentrated vortex core and to reduce the computer time.

2. Description of Present Method

For convenience, Mehrotra's method (Ref. 4) will be called vortex-filament model and the present method the core model. In the present analysis, the basic assumptions are: (1) the wing is represented by a bound vortex sheet, across which there exists a pressure difference;

(2) the separated flow along leading-edges is represented by force-free leading-edge vortex elements which feed vorticity into a concentrated core. During the iteration process, the following boundary conditions are imposed on both vortex-filament and core models: (1) The wing surface must be impermeable; (2) Kutta conditions are imposed along the leading- and trailing-edges of the wing; (3) in the vortex-filament model, force-free condition is applied on the leading-edge vortex filaments and trailing wake elements; (4) in the core model, force-free condition is applied on the free vortex elements, concentrated core and trailing wake elements.

The computational procedures of the present method are as follows:

(1) Establish the leading-edge vortex filament system with Mehrotra's method in two iterations.

(2) Find the centroid of the established leading-edge vortex filament system. Note that to calculate the centroid of the leading-edge vortex filament system, a series of cross flow planes are considered, proceeding from the wing apex toward the trailing-edge. The centroids of the vortex filaments penetrating these planes are given by

$$\bar{y}_j = \frac{\sum_{i=1}^{n_j} \Gamma_i y_{ij}}{\Gamma_{cj}} \tag{1}$$

$$\bar{z}_j = \frac{\sum_{i=1}^{n_j} \Gamma_i z_{ij}}{\Gamma_{cj}} \tag{2}$$

where $\bar{y}_j$, $\bar{z}_j$ are the centroid position in the j^{th} plane,

y_{ij}, z_{ij} are the intersection position of the i^{th} vortex filament with j^{th} plane,

Γ_i is the circulation around the i^{th} vortex filament,

Γ_{cj} is the concentrated line vortex strength at the j^{th} plane,

n_j is the number of vortex filaments penetrating the j^{th} plane.

(3) Allow the leading-edge vortex elements to merge and feed vorticity into the core through connecting segments.

(4) In order to have reasonable starting solution so that computer time can be reduced, the initial z coordinates of concentrated core from step 2 are modified to take the experimental values summarized by Smith (Ref. 5).

$$
\begin{aligned}
z_v &= 0.154\,a + 0.1 \quad , && a < 1.2 \\
z_v &= 0.1333\,a + 0.158 \quad , && 1.2 \leq a < 2.2 \\
z_v &= 0.13\,a + 0.132 \quad , && a \geq 2.2
\end{aligned}
\tag{3}
$$

where,

$$
a = \tan\alpha \,/\, (A/c_r) , \tag{4}
$$

A is the aspect ratio, c_r the root chord, and z_v is the nondimensional z-coordinate of the concentrated core, referring to the local semispan.

(5) During the iteration process, the new locations of the free vortex elements, concentrated core and trailing wake are determined by satisfying the force free condition. Note that the force free condition is not applied on both the feeding segments and the free sheet along the very first vortex strip. The new locations of free vortex elements and the core along the first vortex strip are obtained by linear interpolation.

(6) From the starting solution of the core model, the core is forced to move downward and outward twice, to obtain the force gradients. In each case, relaxation paramters (λ_y, λ_z) for determining new core coordinates are assumed empirically as follows (See step 9):

first time

$$\lambda_{y_1} = -0.05 \left| \frac{\Sigma F_z}{\Sigma F} \right| \tag{5}$$

$$\lambda_{z_1} = -0.25 \cdot \frac{C_{L_s} - C_L}{C_{L_s}} \cdot \frac{\tan 30^\circ}{\tan^2 \alpha} \tag{6}$$

second time

$$\lambda_{z_2} = -0.025 \cdot \frac{\tan 30^\circ}{\tan \alpha} \tag{7}$$

$$\lambda_{y_2} = \lambda_{z_2} \cdot \frac{\lambda_{y_1}}{\lambda_{z_1}} \tag{8}$$

In Eq. (5), ΣF_z is the total force acting on the core in the z direction and ΣF is the total force. In Eq. (6), C_L is the initially calculated lift coefficient and C_{L_s} is the lift coefficient by suction analogy. Note that λ_y and λ_z are assumed constant along the entire core.

(7) In the next iteration, λ_y and λ_z of each segment of core are computed, based on the difference of segment force in the preceeding two iterations.

$$\lambda_{y_i} = C_{y_i} \cdot \left(\frac{F_{z_2} - F_{z_1}}{|F_{z_2}|} \right)_i \quad , \quad |C_{y_i}|_1 = 0.5 \frac{\lambda_{y_1}}{\lambda_{z_1}} \tag{9}$$

$$\lambda_{z_i} = C_{z_i} \left(\frac{F_{y_2} - F_{y_1}}{|F_{y_2}|} \right)_i \quad , \quad |C_{z_i}| = 0.1 \tag{10}$$

where the signs of C_{y_i} and C_{z_i} are the same as those of F_{z2} and F_{y2}, respectively. The physical idea is that the core should be moved in the direction of reducing force magnitude.

(8) The new positions of free vortex elements in each iteration are determined by the following equations,

$$\left(\frac{\Delta y}{\Delta x}\right)' = \frac{V_y}{V_x} \tag{11}$$

$$\left(\frac{\Delta z}{\Delta x}\right)' = \frac{V_z}{V_x} \tag{12}$$

where V_x, V_y, V_z are the total velocity components in the respective coordinate directions. The new slopes of each segment of free vortex elements are

$$\left(\frac{\Delta y}{\Delta x}\right)_{new} = 0.5\left(\frac{\Delta y}{\Delta x}\right)' + 0.5\left(\frac{\Delta y}{\Delta x}\right)_{old} \tag{13}$$

$$\left(\frac{\Delta z}{\Delta x}\right)_{new} = 0.5\left(\frac{\Delta z}{\Delta x}\right)' + 0.5\left(\frac{\Delta z}{\Delta x}\right)_{old} \tag{14}$$

Since the length of each segment is conserved, therefore

$$\Delta s = \Delta x\sqrt{1+\left(\frac{\Delta y}{\Delta x}\right)^2+\left(\frac{\Delta z}{\Delta x}\right)^2} \tag{15}$$

$$(\Delta x)_{new} = \frac{\Delta s}{\sqrt{1+\left(\frac{\Delta y}{\Delta x}\right)^2_{new}+\left(\frac{\Delta z}{\Delta x}\right)^2_{new}}} \tag{16}$$

It follows that

$$(\Delta y)_{new} = (\Delta x)_{new}\cdot\left(\frac{\Delta y}{\Delta x}\right)_{new} \tag{17}$$

$$(\Delta z)_{new} = (\Delta x)_{new}\cdot\left(\frac{\Delta z}{\Delta x}\right)_{new} \tag{18}$$

Thus, the new position of free vortex sheet are found as follows,

$$x_{i\,new} = x_i + \Delta x_{new} \tag{19}$$

$$y_{i\,new} = y_i + \Delta y_{new} \tag{20}$$

$$z_{i\,new} = z_i + \Delta z_{new} \tag{21}$$

(9) During each iteration, the Joukowsky force acting on each segment of the core is computed. Let

$$\vec{F} = \vec{v} \times \vec{\Gamma} = (V_x i + V_y j + V_z k) \times (\Gamma_1 i + \Gamma_2 j + \Gamma_3 k) \tag{22}$$

Then,

$$\frac{F_y}{\Gamma_1 V_x} = \frac{V_z}{V_x} - \frac{\Gamma_3}{\Gamma_1} = \frac{V_z}{V_x} - \frac{\Delta z}{\Delta x} \tag{23}$$

$$\frac{F_z}{\Gamma_1 V_x} = \frac{\Gamma_2}{\Gamma_1} - \frac{V_y}{V_x} = \frac{\Delta y}{\Delta x} - \frac{V_y}{V_x} \tag{24}$$

If the new position of the core is such that $F_y = 0$ and $F_z = 0$, then

$$0 = \left(\frac{V_z}{V_x}\right)' - \left(\frac{\Delta z}{\Delta x}\right)' \tag{25}$$

$$0 = \left(\frac{\Delta y}{\Delta x}\right)' - \left(\frac{V_y}{V_x}\right)' \tag{26}$$

Assume that

$$\frac{V_z}{V_x} \approx \left(\frac{V_z}{V_x}\right)'$$

$$\frac{V_y}{V_x} \approx \left(\frac{V_y}{V_x}\right)'$$

Combining Eqs. (23), (25) and (24), (26) yields the following equation for the i^{th} segment:

$$\left(\frac{\Delta y}{\Delta x}\right)_i' = \left(\frac{\Delta y}{\Delta x}\right)_{old} - \frac{F_{zi}}{\Gamma_{ic} V_{xi}} \tag{27}$$

$$\left(\frac{\Delta z}{\Delta x}\right)_i' = \left(\frac{\Delta z}{\Delta x}\right)_{old} + \frac{F_{yi}}{\Gamma_{ic} V_{xi}} \tag{28}$$

Then new slopes of i^{th} segment of concentrated core are determined by:

$$\left(\frac{\Delta y}{\Delta x}\right)_{new} = (1-\lambda_y)\left(\frac{\Delta y}{\Delta x}\right)_{old} + \lambda_y \left(\frac{\Delta y}{\Delta x}\right)_i' \tag{29}$$

$$\left(\frac{\Delta z}{\Delta x}\right)_{new} = (1-\lambda_z)\left(\frac{\Delta z}{\Delta x}\right)_{old} + \lambda_z \left(\frac{\Delta z}{\Delta x}\right)_i' \tag{30}$$

Combining Eqs. (27) through (30) results in

$$\left(\frac{\Delta y}{\Delta x}\right)_{new} = \left(\frac{\Delta y}{\Delta x}\right)_{old} - \lambda_y \frac{F_{zi}}{\Gamma_{ic} V_{xi}} \tag{31}$$

$$\left(\frac{\Delta z}{\Delta x}\right)_{new} = \left(\frac{\Delta z}{\Delta x}\right)_{old} + \lambda_z \frac{F_{yi}}{\Gamma_{ic} V_{xi}} \tag{32}$$

Since the segment length is conserved, it follows that

$$\Delta S = \Delta x \sqrt{1 + \left(\frac{\Delta y}{\Delta x}\right)^2 + \left(\frac{\Delta z}{\Delta x}\right)^2} \tag{33}$$

$$(\Delta x)_{new} = \frac{\Delta s}{\sqrt{1+\left(\frac{\Delta y}{\Delta x}\right)^2_{new}+\left(\frac{\Delta z}{\Delta x}\right)^2_{new}}} \tag{34}$$

Hence,

$$(\Delta y)_{new} = (\Delta x)_{new} \cdot \left(\frac{\Delta y}{\Delta x}\right)_{new} \tag{35}$$

$$(\Delta z)_{new} = (\Delta x)_{new} \cdot \left(\frac{\Delta z}{\Delta x}\right)_{new} \tag{36}$$

Thus, the new positions of concentrated core are found as follows,

$$x_{i\,new} = x_i + \Delta x_{new} \tag{37}$$

$$y_{i\,new} = y_i + \Delta y_{new} \tag{38}$$

(10) The new positions fo trailing wake in each iteration are determined in the same manner as described in Ref. 4.

Note that the segment length is preserved along the free vortex sheet, concentrated core and trailing wake. In addition, the effect of the secondary vortices has not been included in the present analysis.

3. Numerical Results

To show the improvement, those cases shown in Ref. 4 were re-calculated and compared in Figures 1 through 12. The following observations can be made:

(1) For the over-all aerodynamic characteristics (Figures 1 through 5), the results from both methods are similar, except that the present results are slightly more accurate at high angles of attack.

(2) There are significant improvements in the predicted ΔC_p distribution, in particular, at moderate to high angles of attack. Difficulty exists at low angles of attack, because free vortex sheets from Mehrotra's model are relatively flat and the initial configurations in the present model are more difficult to determine.

In most cases, final results can be obtained with two iterations in Mehrotra's model and three iterations in the present model. The computer time is approximately reduced by half as compared with Ref. 4.

4. References

(1) Weber, J. A., Brune, G. W., Johnson, F. T., Lu, P. and Rubbert, P. E., "Three-Dimensional Solution of Flows over Wings with Leading-Edge Vortex Separation," AIAA Journal, Vol. 14, April 1976, pp. 519-525.

(2) Johnson, F. T., Tinoco, E. N., Lu, P. and Epton, M. A., "Recent Advances in the Solution of Three-Dimensional Flows over Wings with Leading Edge Vortex Separation," AIAA Paper 79-0282, 1979.

(3) Kandil, O. A., Mook, D. T. and Nayfeh, A. H., "Nonlinear Prediction of the Aerodynamic Loads on Lifting Surfaces," Journal of Aircraft, Vol. 13, Jan. 1976, pp. 22-28.

(4) Mehrotra, S. C. and Lan, C. E., "A Theoretical Investigation of the Aerodynamics of Low-Aspect-Ratio Wings with Partial Leading-Edge Separation," NASA CR-145304, January 1978.

(5) Smith, J. H. B., "Improved Calculation of Leading-Edge Separation from Slender, Thin, Delta Wings," Proc. Roy. Soc. A. 306, pp. 67-90, 1968.

(6) Fink, P. T., "Wind-Tunnel Tests on a Slender Delta Wing at High Incidence," Z. Flugwissenschaften, Jahrg. 4, Heft 7, pp. 247-249, July 1956.

(7) Wentz, W. H., "Effects of Leading-Edge Camber on Low-Speed Characteristics of Slender Delta Wings," NASA CR-2002, 1972.

(8) Bartlett, G. E. and Vidal, R. J., "Experimental Investigation of Influence of Edge Shape on the Aerodynamic Characteristics of Low-Aspect-Ratio Wings at Low-Speeds," Journal of Aeronautical Science, Vol. 22, No. 8, pp. 517-533, Aug. 1955.

(9) Fink, P. T. and Taylor, J., "Some Low Speed Experiments with 20 deg. Delta Wings," ARC R & M 3489, 1967.

(10) Marsden, D. J., Simpson, R. W. and Rainbird, W. J., "The Flow over Delta Wings at Low Speeds with Leading-Edge Separation," The College of Aeronautics, Cranfield, Rept. No. 114, Feb. 1958.

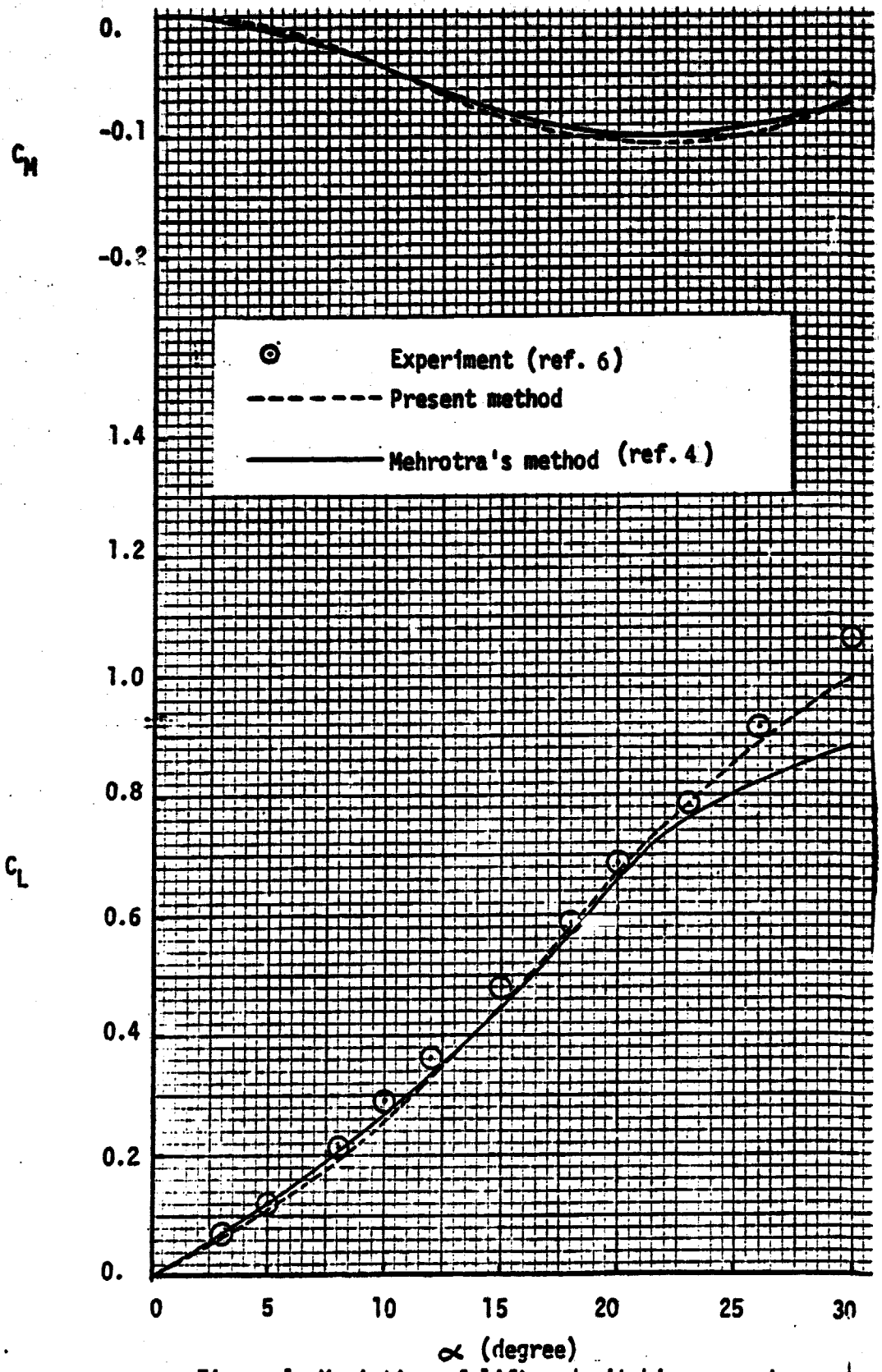

Figure 1. Variation of lift and pitching moment (about 0.25 $\bar{C}$) coefficients with angle of attack for AR = 0.7053 delta wing

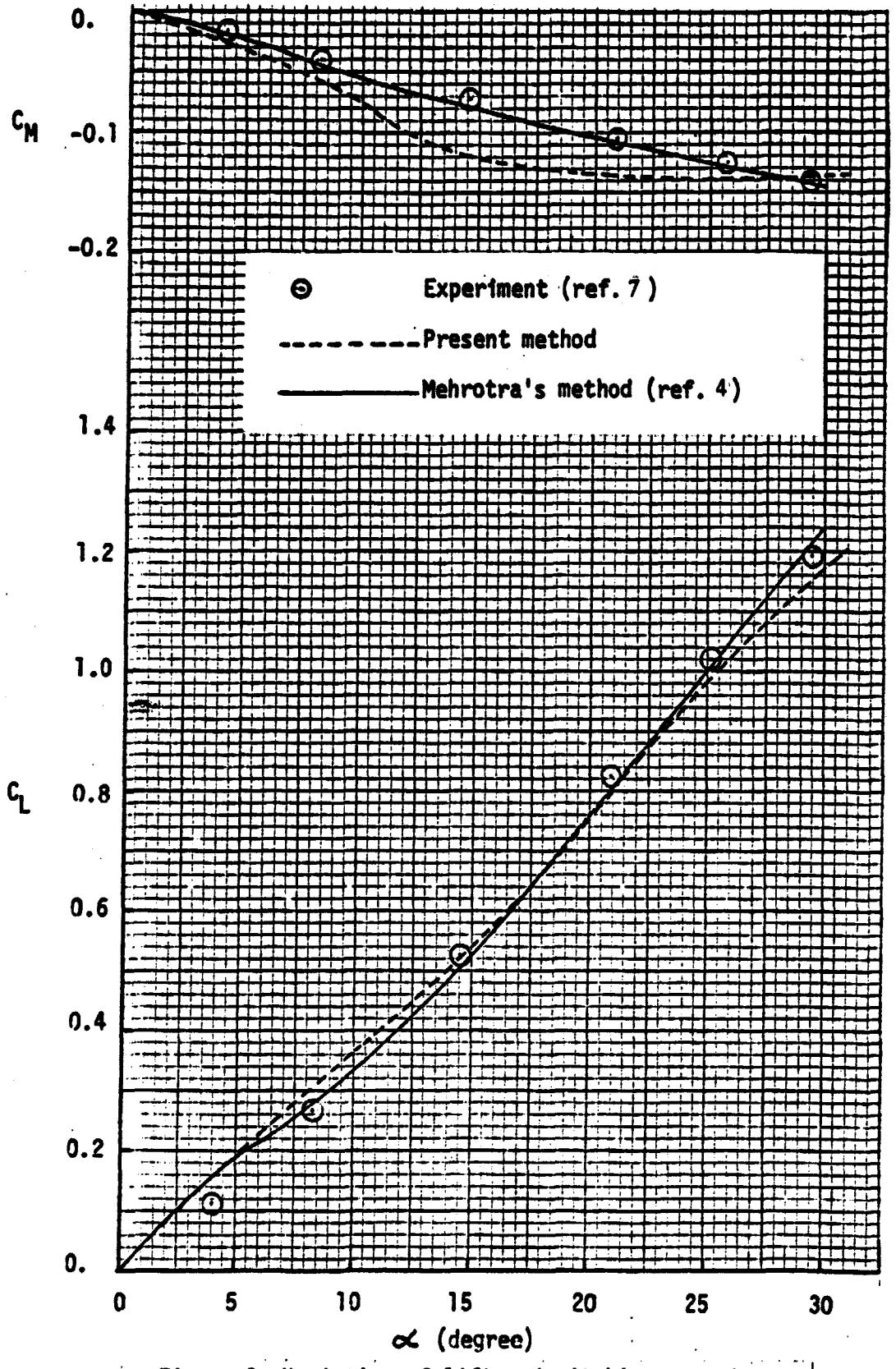

Figure 2. Variation of lift and pitching moment (about 0.25 $\bar{C}$) coefficients with angle of attack for AR = 1.147 delta wing

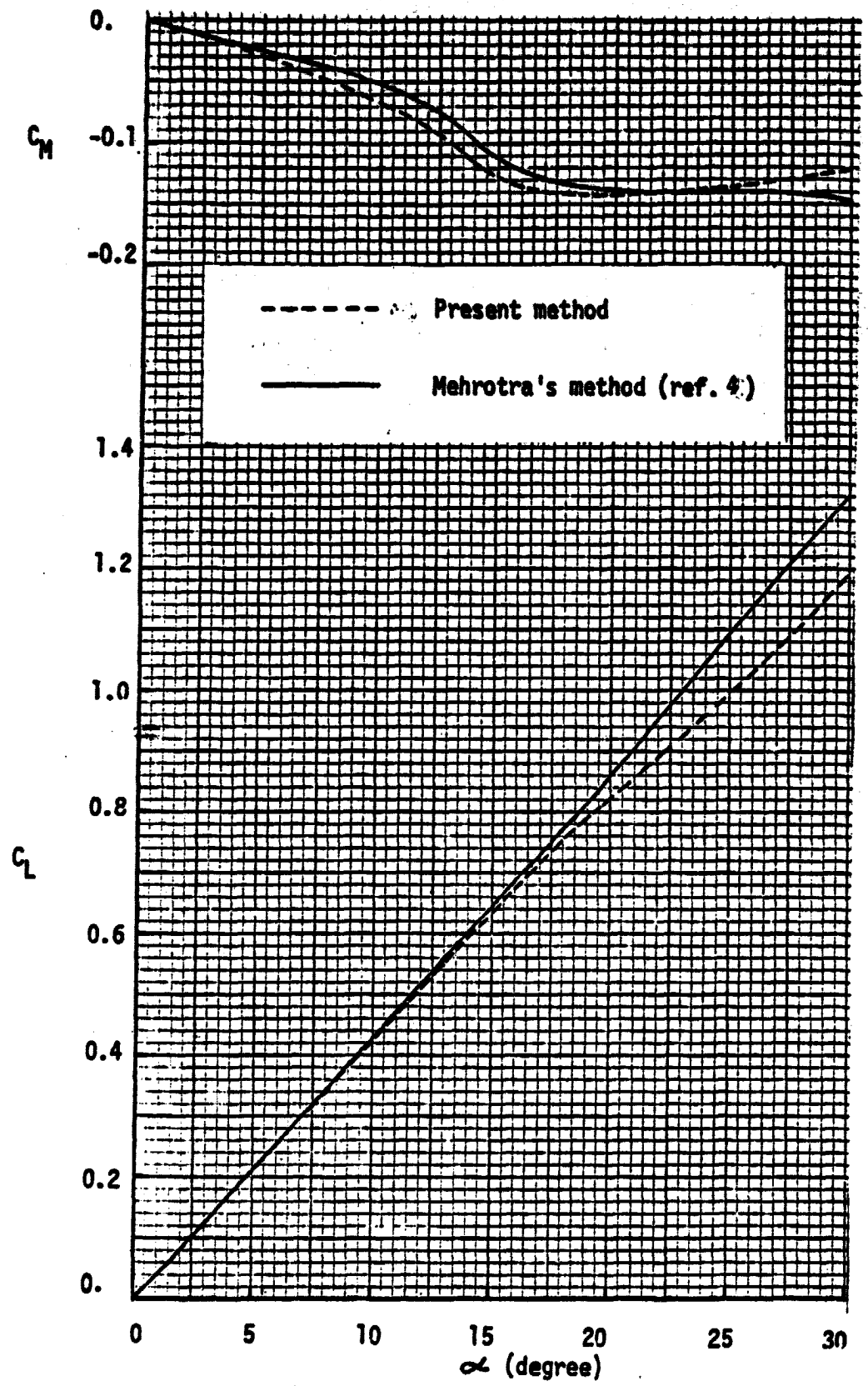

Figure 3. Variation of lift and pitching moment (about 0.25 $\bar{C}$) coefficients with angle of attack for AR = 1.4559 delta wing

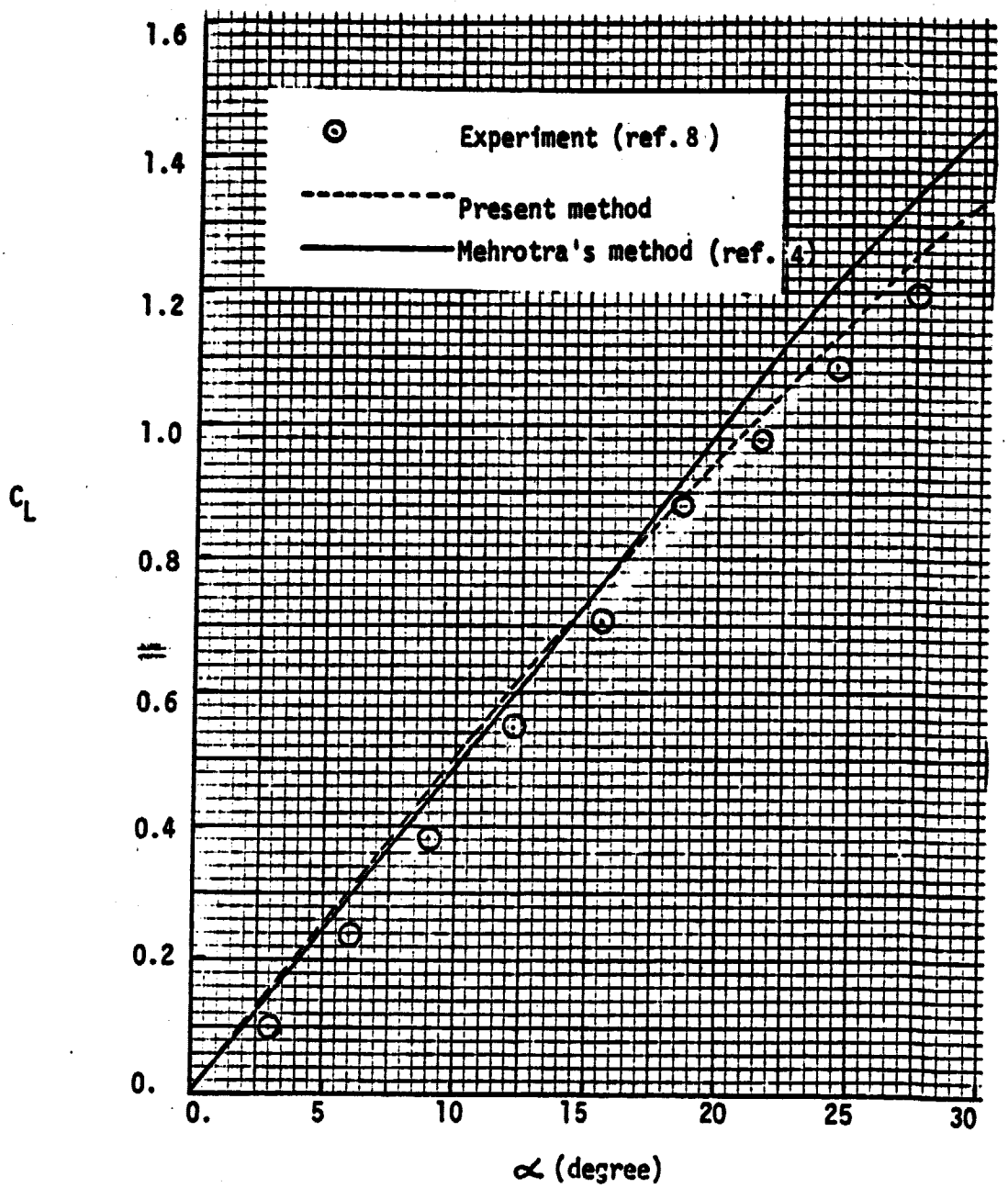

Figure 4. Variation of lift coefficient with angle of attack for AR = 2.0 delta wing

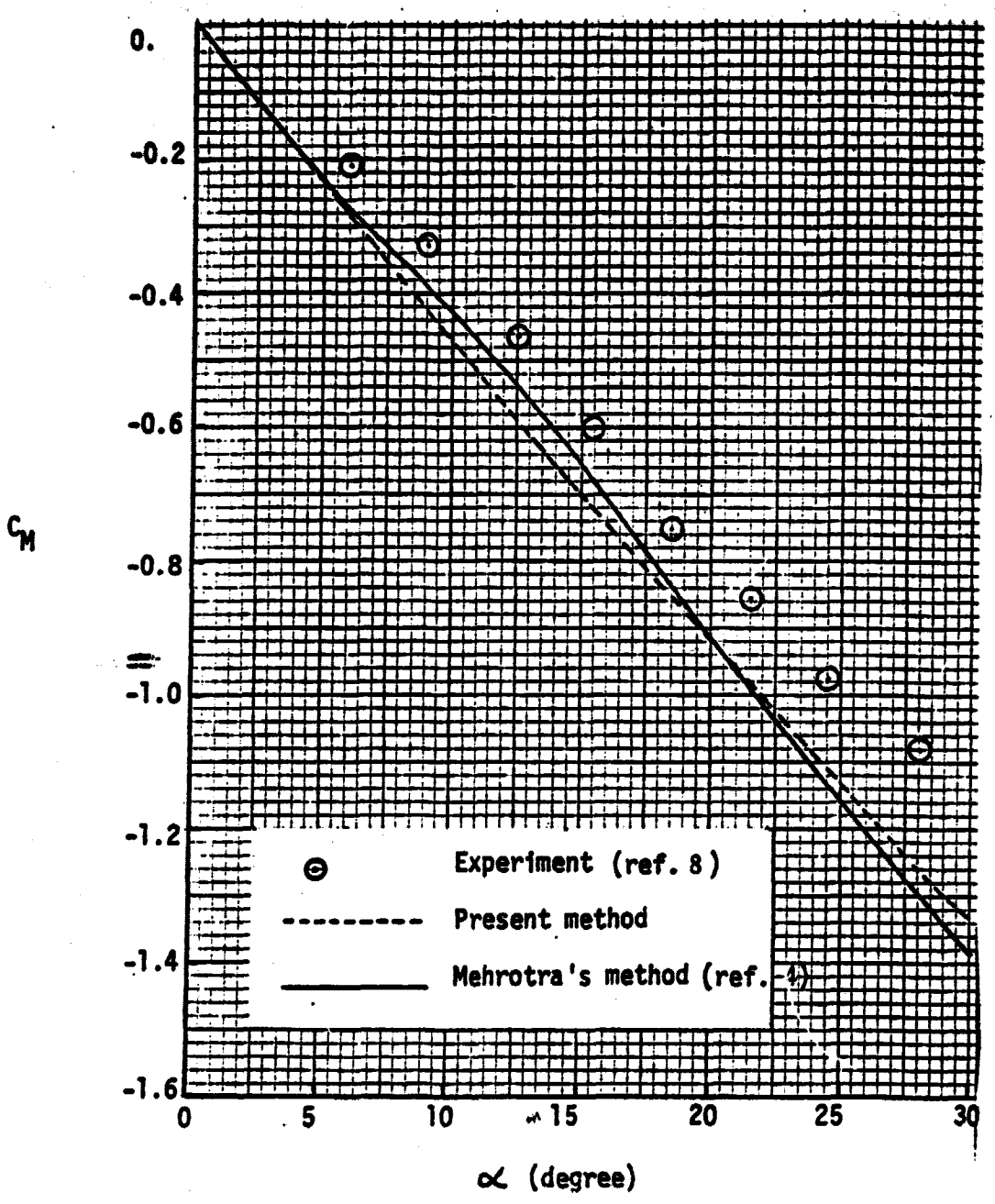

Figure 5. Variation of pitching moment (about apex) coefficient with angle of attack for AR = 2.0 delta wing

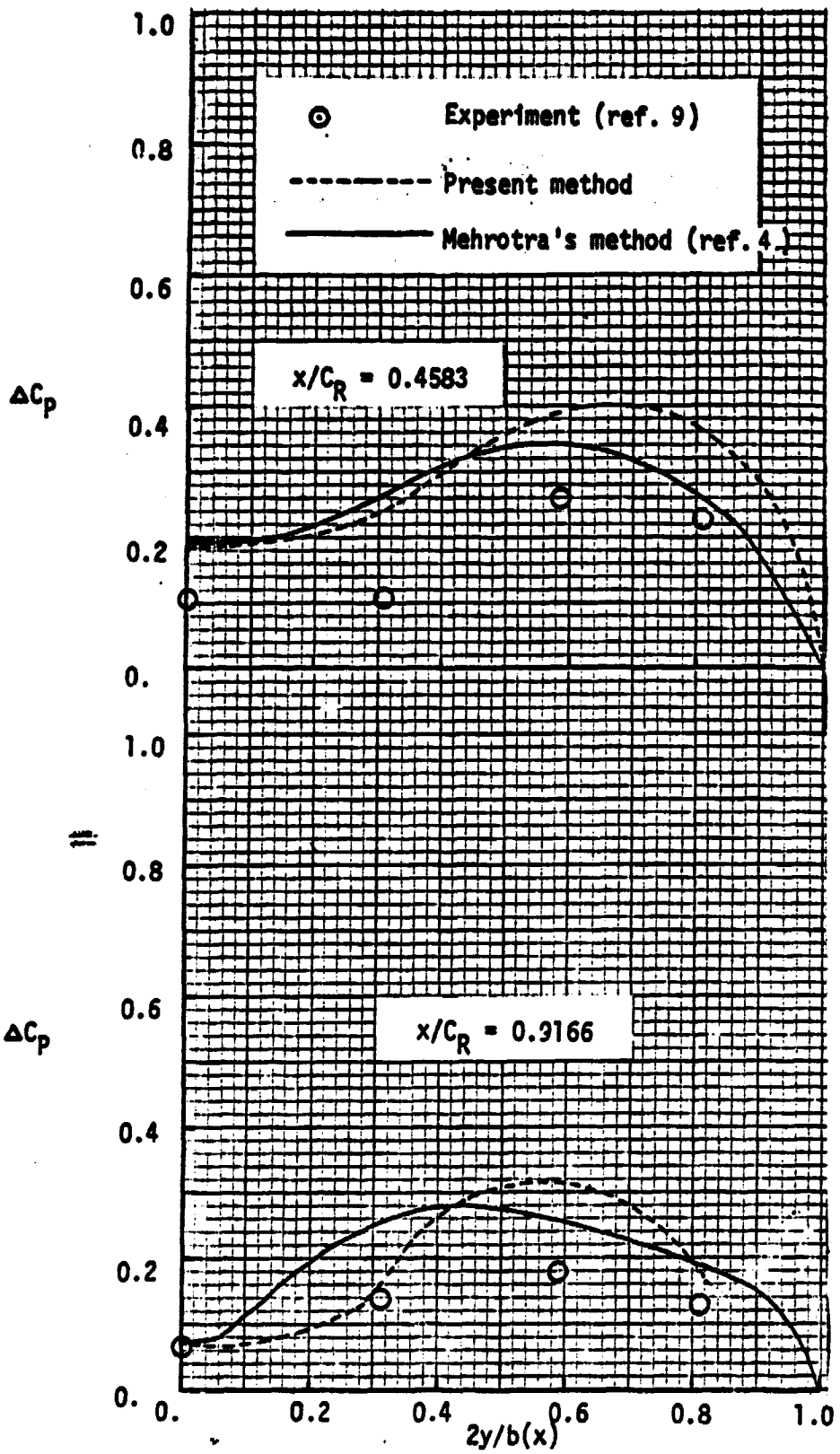

Figure 6. Pressure distribution for AR = 0.7053 delta wing at 10.0 degree angle of attack

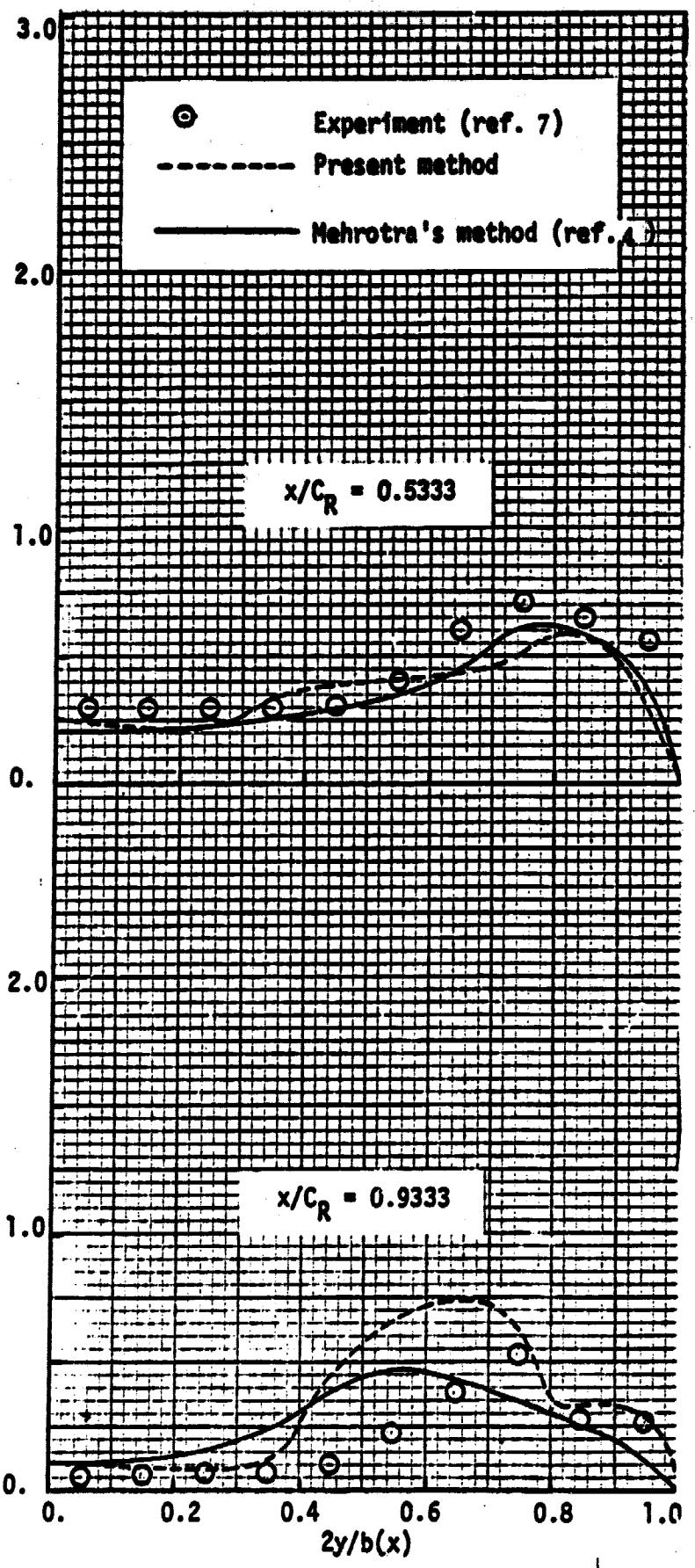

Figure 7. Pressure distribution for AR = 1.147 delta wing at 10.2 degree angle of attack

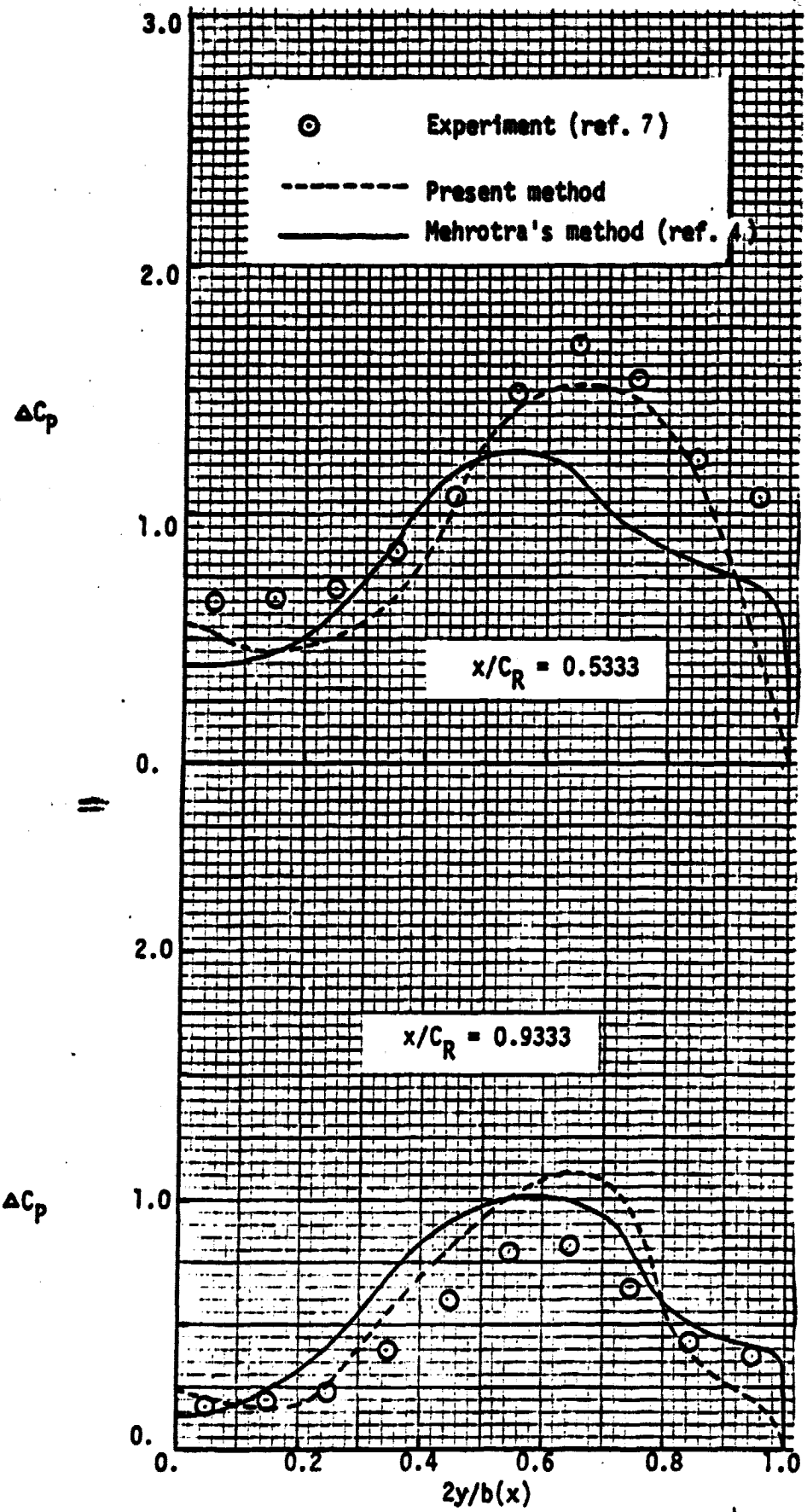

Figure 8. Pressure distribution for AR = 1.147 delta wing at 20.4 degree angle of attack

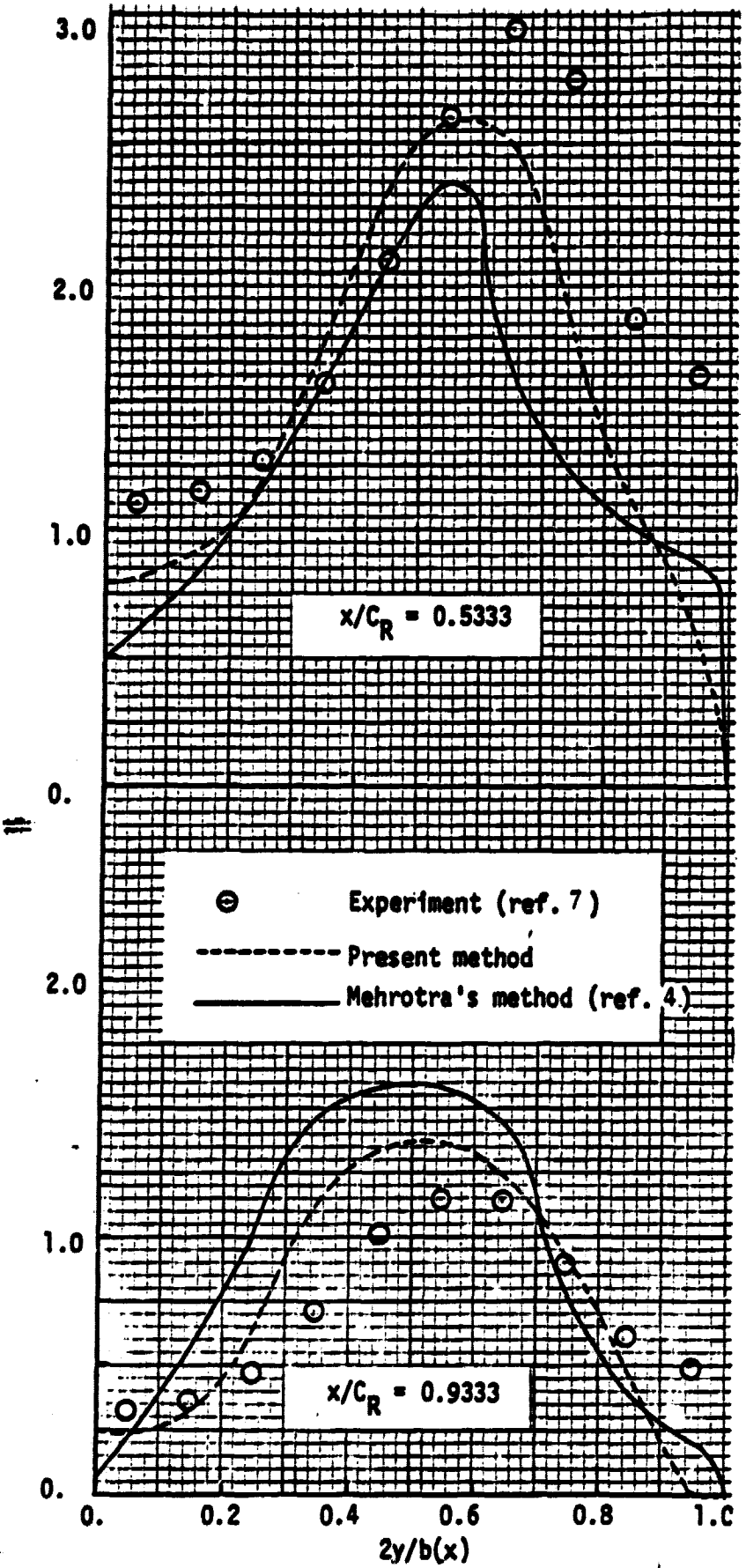

Figure 9. Pressure distribution for AR = 1.147 delta wing at 30.7 degree angle of attack

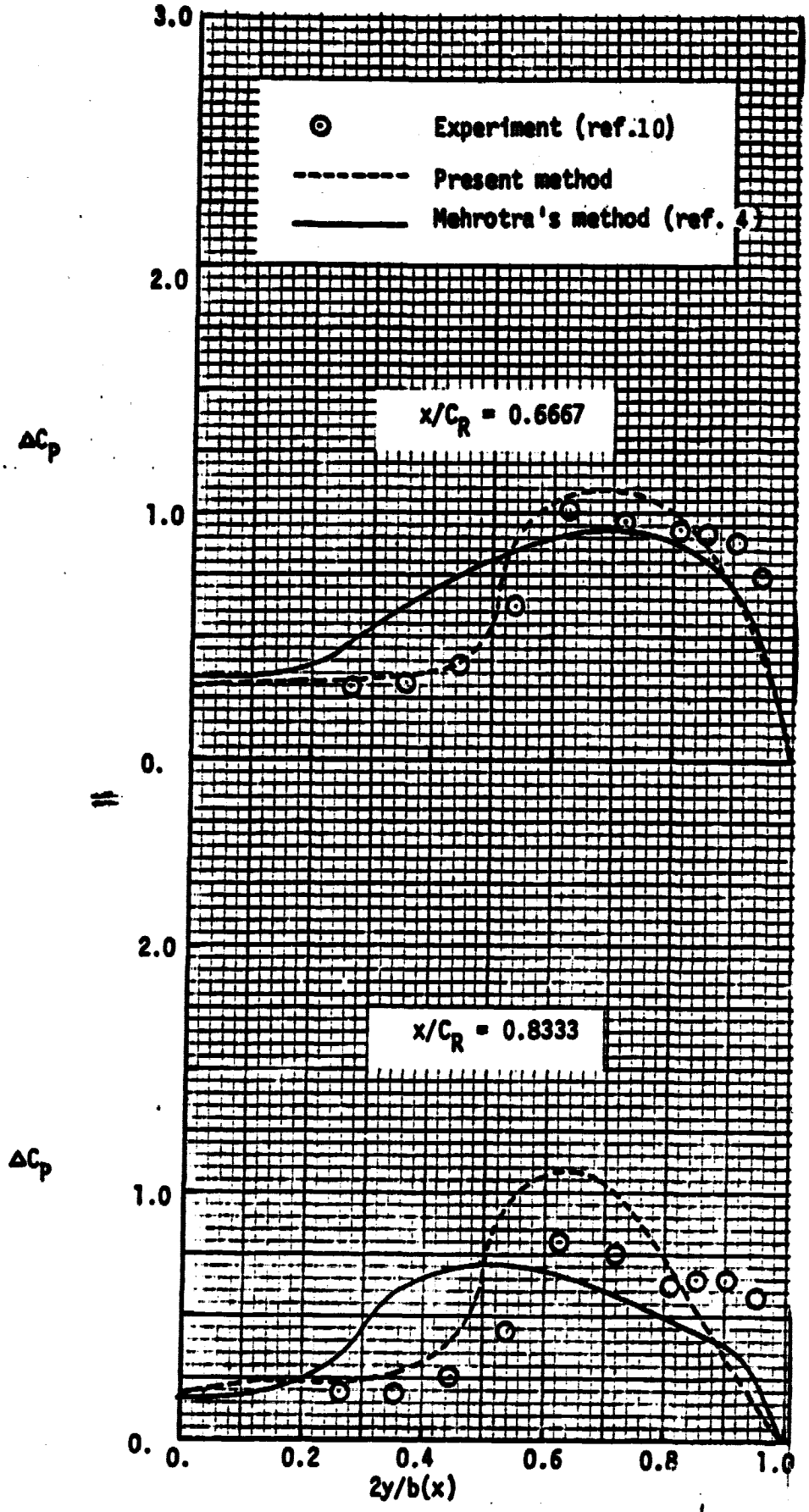

Figure 10. pressure distribution for AR = 1.4559 delta wing at 14.0 degree angle of attack

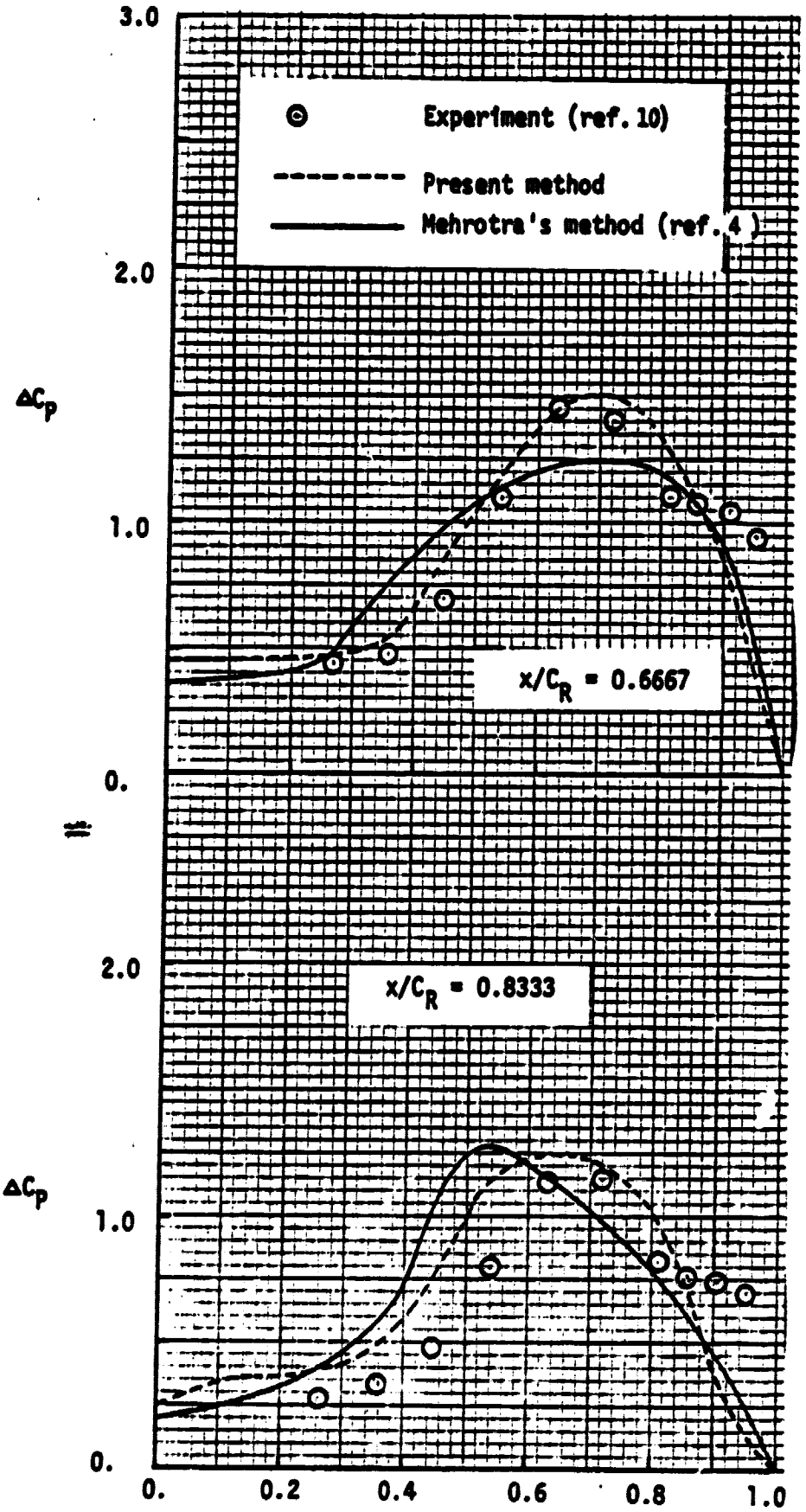

Figure 11. Pressure distribution for AR = 1.4559 delta wing at 19.1 degree angle of attack

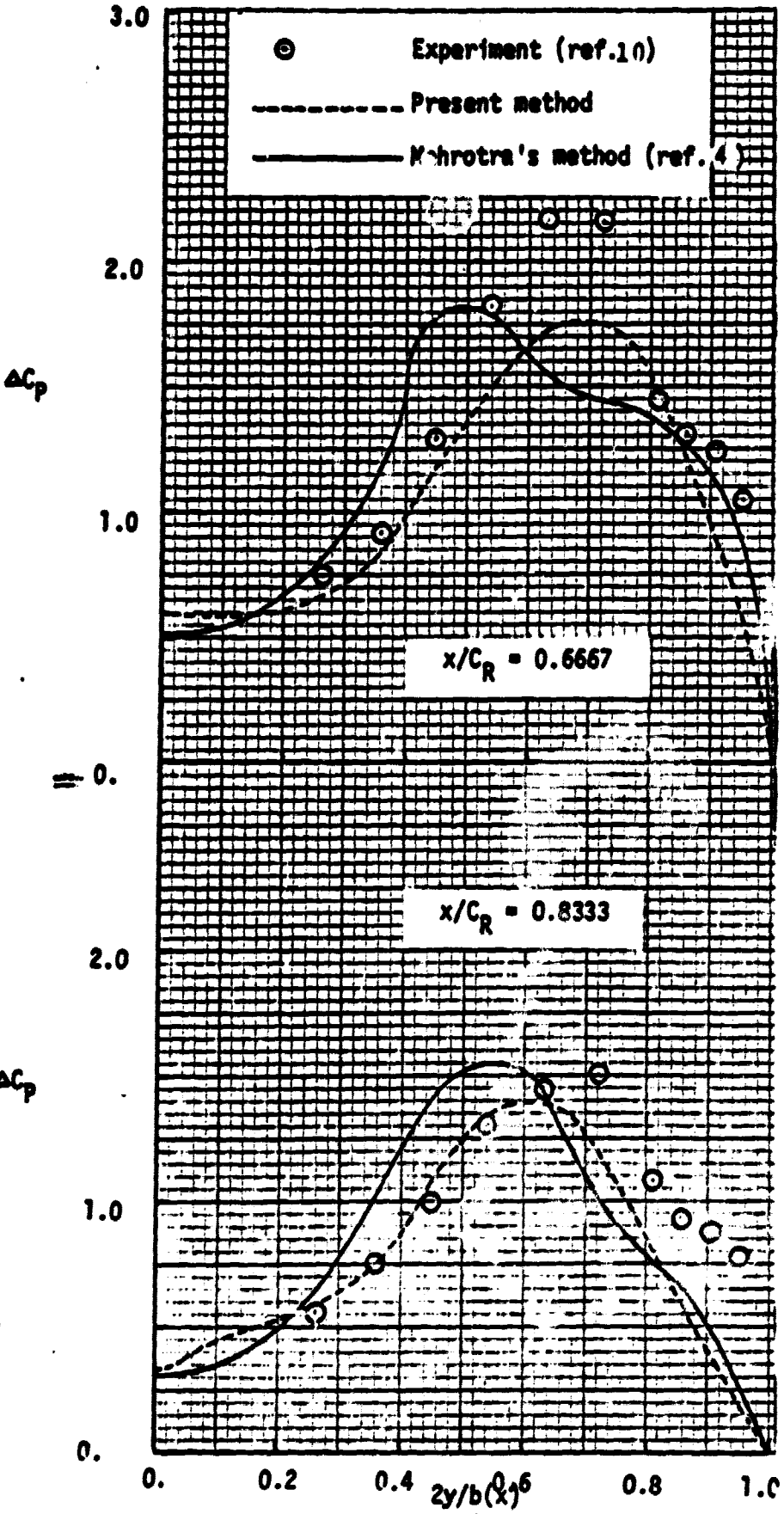

Figure 12. Pressure distribution for AR = 1.4559 delta wing at 23.9 degree angle of attack